ESTIMATING THE ELASTIC MODULI OF TRANSVERSELY ISOTROPIC FORMATIONS

by

K. J. Ellefsen and C. H. Cheng

Earth Resources Laboratory
Department of Earth, Atmospheric, and Planetary Sciences
Massachusetts Institute of Technology
Cambridge, MA 02139

ABSTRACT

Using acoustic logging data, we develop a method of estimating the horizontal shear modulus c_{66}) of a transversely isotropic formation with its axis of symmetry parallel to that of the borehole. The data for the inversion are the wavenumbers, at every frequency, of the guided waves. The inversion minimizes the difference between these observed wavenumbers and those calculated by a forward model. The final estimates of the elastic moduli are constrained by the *a priori* estimates of their values and by the requirement to keep the stiffness tensor positive definite. The inversion produced similar results when it was applied to synthetic data from hard and soft formations. The estimate for the shear modulus, c_{66}, was fairly accurate because this parameter is moderately well resolved. The estimates for c_{11} and c_{13} are inaccurate because they are poorly resolved by the data. Tight constraints on the fluid modulus prevent this parameter from changing much. The inversion did not attempt to estimate either c_{33} or c_{44} because they can be determined from the refracted P- and S-waves or the flexural wave.

INTRODUCTION

Knowledge of the elastic properties of a formation is important in the earth sciences and the petroleum industry. In the Ocean Drilling Project, Poisson's ratio is used to predict the lithification of sediments and as a marker for specific formations. In industry, these constants are used to correlate acoustic logging and seismic data, which is necessary for reservoir characterization and stratigraphic analysis. They are also used to estimate the strength of a formation — an important parameter which determines how a formation is fractured and whether a formation might collapse during production. Since these applications require closely spaced estimates of the elastic properties, the estimates are often made with acoustic logging measurements because of the small wavelengths

of the elastic waves used.

Several years ago, most sedimentary rocks were considered to be isotropic, meaning that their elastic properties are characterized by only two constants, the bulk and shear moduli. When logging in hard formations, the velocities of the refracted P- and S-waves and the density logs were enough information to determine these moduli. In soft formations, the refracted S-wave does not exist, but the shear modulus can be determined from the tube and leaky P waves (Cheng et al., 1982; Stevens and Day, 1986; Cheng, 1987; Meredith et al., 1989).

Recent evidence (see e.g., Thomsen, 1986 and Winterstein, 1985) suggests that many sedimentary rocks are actually transversely isotropic, which means the elastic properties are characterized by five constants: c_{11}, c_{13}, c_{33}, c_{44}, and c_{66}. White and Tongtaow (1981) and Chan and Tsang (1983), who investigated acoustic logging in transversely isotropic media, found that the velocities of the refracted P- and S-waves are $\sqrt{c_{33}/\rho}$ and $\sqrt{c_{44}/\rho}$, respectively, where ρ is the formation density. Consequently, the refracted waves can be used to estimate these two moduli. The important problem then is developing a method to estimate the other moduli. White and Tongtaow discovered that the only elastic modulus which affects the tube wave velocity at 0 Hz is c_{66}. This fact suggest that the guided waves might be used to estimate some of the unknown moduli as these waves are used in isotropic formations to estimate the shear modulus.

In this paper, we describe a method of estimating the horizontal shear modulus, c_{66}, of a transversely isotropic formation using the wavenumbers of the guided waves. We develop a robust procedure and apply it to synthetic data from hard and soft formations. These two cases establish how accurately c_{66} can be estimated and why c_{11} and c_{13} cannot be determined with this procedure.

METHOD

Formulation

The model consists of a fluid-filled borehole through a transversely isotropic formation, the axis of which coincides with that of the borehole (Figure 1). The properties of the formation are described by five elastic moduli and density; the properties of the fluid by one modulus and density. For the synthetic examples in this paper, a tool is not present, although it must be included when analyzing field data. The formation is assumed to be homogeneous which implies that the formation has been neither extensively damaged by drilling nor altered by shale swelling. The permeability must be small to make its effects upon the guided waves negligible (Rosenbaum, 1974). The viscosity of the fluid can be ignored (Burns, 1988), and the effects of azimuthal

anisotropy are assumed to be unimportant. The borehole wall is cylindrical because small perturbations from the cylindrical shape, which always exist in field situations, have a minor effect upon the phase velocity of the guided waves (Ellefsen and Cheng, 1989).

The forward model for the inversion is based upon the period equation. Using expressions for displacements and stress in a transversely isotropic solid (Tongtaow, 1982), boundary conditions at the fluid-formation interface are used to derive the period equation. This equation incorporates all of the information about the formation and fluid in terms of elastic constants and densities and about the guided wave in terms of its wavenumber and frequency. The period equation is solved numerically at each frequency for a wavenumber when it exists.

The inversion, which selects appropriate elastic constants for the formation and fluid, is based upon a cost function that has three terms. The first term contributes information about the data, the second about the original estimates of the elastic moduli, and the third about the physical constraints on the moduli. These three terms will now be developed.

The first term in the cost function requires that the wavenumbers predicted by the forward model closely match the observed wavenumbers. Array processing of microseismograms from multi-receiver tools yields, in the frequency domain, estimates of the wavenumber and the amplitude for each guided wave (Ellefsen et al., 1987). For the inversion the wavenumbers are arranged in a vector denoted $\mathbf{d}_{obs}$. The amplitude of the guided wave is roughly proportional to the accuracy of the wavenumber estimate and is used to develop a data covariance matrix, $\mathbf{C}_D$, which is diagonal because all wavenumber estimates are assumed to be independent. The predicted wavenumbers are arranged in a vector denoted $\mathbf{g}(\mathbf{m})$, where $\mathbf{m}$ represents the model parameters (i.e., the elastic moduli). In terms of probability theory, the relationship between the observed and predicted wavenumbers may be expressed by the generalized Gaussian density function:

$$f_p(\mathbf{m}) = K_1 \exp\left[-\frac{1}{p}(|\mathbf{d}_{obs} - \mathbf{g}(\mathbf{m})|^{p/2})^T \mathbf{C}_D^{-1}(|\mathbf{d}_{obs} - \mathbf{g}(\mathbf{m})|^{p/2})\right] \quad , \tag{1}$$

(Tarantola, 1987) where K_1 is a normalizing constant. The important property of $f_p(\mathbf{m})$ is that when p is close to 1 $f_p(\mathbf{m})$ decreases slowly away from its maximum value at $\mathbf{d}_{obs} = \mathbf{g}(\mathbf{m})$. Hence, a few observed wavenumbers can deviate significantly from their correct value without seriously affecting the solution. This property makes the inversion robust. Maximizing the probability density function is equivalent to minimizing the negative of its exponent,

$$\frac{1}{p}(|\mathbf{d}_{obs} - \mathbf{g}(\mathbf{m})|^{p/2})^T \mathbf{C}_D^{-1}(|\mathbf{d}_{obs} - \mathbf{g}(\mathbf{m})|^{p/2}) \quad , \tag{2}$$

which will be the first term in the cost function.

	c_{13}	c_{33}	c_{44}	c_{66}
c_{11}	0.37	0.95	0.83	0.89
c_{13}		0.28	-0.090	0.022
c_{33}			0.88	0.85
c_{44}				0.95

Table 1: Correlation coefficients between the elastic moduli of transversely isotropic rocks.

The second term in the cost function requires that the elastic constants obtained by the inversion be close to the initial estimates of their values. Because c_{33} can be determined from the refracted P-wave and c_{44} from either the refracted S-wave or flexural wave, the values for these moduli are fixed during the inversion. Thomsen (1986) tabulated 44 laboratory and field measurements of the elastic moduli for transversely isotropic rocks; cross-plots (Figure 2) show that, when c_{33} and c_{44} are given, the ranges of values for c_{11}, c_{13}, and c_{66} are well defined. Notice that c_{13} depends strongly on the linear combination, $c_{33} - 2c_{44}$. (To understand this result, assume for a moment that the rock is isotropic. The elastic moduli in terms of the Lamé parameters are $c_{11} = c_{33} = \lambda + 2\mu$, $c_{13} = \lambda$, and $c_{44} = c_{66} = \mu$. For a rock which is only slightly anisotropic, $c_{33} - 2c_{44}$ is close to c_{13}.) The most-likely value for each modulus is approximately in the middle of its range and will be called the *a priori* model parameter. For the inversion, these parameters are placed in a vector denoted $\mathbf{m}_o$. The initial model covariance matrix, $\mathbf{C}_M$, is calculated from the standard deviations of the model parameters, which are estimated from the cross-plots, and from the correlation coefficients between the moduli, which were calculated from Thomsen's data and are listed in Table 1. The modulus for the fluid is uncorrelated with the moduli for the formation. The relationship between the initial model parameters and those predicted by the inversion may be expressed by the normal density function:

$$\rho_M(\mathbf{m}) = K_2 \exp\left[-\frac{1}{2}(\mathbf{m}-\mathbf{m}_o)^T \mathbf{C}_M^{-1}(\mathbf{m}-\mathbf{m}_o)\right] \tag{3}$$

where K_2 is a normalizing constant. Maximizing this density function is equivalent to minimizing the negative of its exponent,

$$\frac{1}{2}(\mathbf{m}-\mathbf{m}_o)^T \mathbf{C}_M^{-1}(\mathbf{m}-\mathbf{m}_o) \quad , \tag{4}$$

which will be the second term in the cost function.

The third term in the cost function requires that the elastic moduli be physically possible. The elastic strain energy density, $\frac{1}{2}e_{ij}c_{ijkl}e_{kl}$, is always positive for any

nonzero strain, e_{ij}. Hence, the tensor of elastic moduli, c_{ijkl}, must be positive definite. For a transversely isotropic medium, a sufficient set of equations to insure positive definiteness are

$$c_{11} - |c_{11} - 2c_{66}| > 0 \quad , \tag{5}$$

$$(c_{11} - c_{66})c_{33} - c_{13}^2 > 0 \quad , \tag{6}$$

and

$$c_{44} > 0 \tag{7}$$

(Auld, 1973). These three equations, which are written symbolically as $h_i(\mathbf{m}) > 0$ (where i is an equation index), are used to develop penalty functions,

$$\psi_i = \frac{\alpha_i}{h_i(\mathbf{m})} \quad , \tag{8}$$

where α_i is a small, positive constant (Bard, 1974). For acceptable values of the elastic moduli, the penalty function is negligibly small. As $h_i(\mathbf{m})$ approaches zero, the penalty function becomes very large forcing the current estimate of the model parameters to remain within the acceptable region. The penalty functions are written in vector form as $\mathbf{\Psi}$, and the inner product,

$$\mathbf{\Psi}^T\mathbf{\Psi} \quad , \tag{9}$$

is the third term in the cost function.

The cost function used by the inversion combines the expressions in 2, 4, and 9:

$$\begin{aligned} \Phi(\mathbf{m}) \quad = \quad & \frac{1}{p}(|\mathbf{d}_{obs} - \mathbf{g}(\mathbf{m})|^{p/2})^T\mathbf{C}_D^{-1}(|\mathbf{d}_{obs} - \mathbf{g}(\mathbf{m})|^{p/2}) + \\ & \frac{1}{2}(\mathbf{m} - \mathbf{m}_o)^T\mathbf{C}_M^{-1}(\mathbf{m} - \mathbf{m}_o) + \mathbf{\Psi}^T\mathbf{\Psi} \quad . \end{aligned} \tag{10}$$

This cost function is minimized with respect to $\mathbf{m}$ to find the best choice for the elastic moduli of the formation and fluid.

Optimization Technique

An approximate technique is used to perform the l_p optimization of the cost function (equation 10). The differences between the observed and predicted wavenumbers are the residuals: $r_i = (d_i)_{obs} - g_i(\mathbf{m})$. A diagonal weighting matrix, $\mathbf{W}$, is defined from these residuals:

$$W_{ii} = \begin{cases} p(\epsilon/|r_i|)^{2-p} & \text{if } |r_i| > \epsilon \\ 1 & \text{if } |r_i| \leq \epsilon \end{cases} \tag{11}$$

where ϵ is a small positive constant and $1 \leq p \leq 2$ (Scales and Gersztenkorn, 1988). The cost function is now rewritten as

$$\Phi(\mathbf{m}) = \frac{1}{p}(|\mathbf{d}_{obs} - \mathbf{g}(\mathbf{m})|^{p/2})^T \mathbf{W}^{-1/2} \mathbf{C}_D^{-1} \mathbf{W}^{-1/2} (|\mathbf{d}_{obs} - \mathbf{g}(\mathbf{m})|^{p/2}) + \frac{1}{2}(\mathbf{m} - \mathbf{m}_o)^T \mathbf{C}_M^{-1} (\mathbf{m} - \mathbf{m}_o) + \boldsymbol{\Psi}^T \boldsymbol{\Psi} \quad . \tag{12}$$

This equation shows that $\mathbf{W}$ prevents large residuals from significantly increasing the cost function and adversely affecting the inversion. The advantage of this formulation is that standard least-squares algorithms can be used to perform the optimization.

The cost function is minimized using a Levenburg-Marquardt algorithm which has been developed for nonlinear, least-squares problems (Moré, 1978; Moré et al., 1980). The Jacobian matrix, which is required for this algorithm, is calculated using a perturbative method (Ellefsen and Cheng, 1989) which is usually more accurate than numerical differentiation. When the inversion obtains a good solution, the costs associated with the constraints are virtually zero. If the product $1/p\mathbf{W}^{1/2}\mathbf{C}_D\mathbf{W}^{1/2}$ is interpreted as a corrected data covariance matrix, then the optimization is like the maximum likelihood inversion (Aki and Richards, 1980).

Interpreting the Results

Three different methods are used to interpret the results of the inversion. First, the final standard deviations for the model parameters are compared to the initial deviations. If a deviation has been significantly reduced, then the corresponding model parameter is well resolved. The final deviations are calculated from the final model covariance matrix,

$$\mathbf{C}_{M'} \approx \left(\mathbf{G}^T \mathbf{C}_D^{-1} \mathbf{G} + \mathbf{C}_M^{-1}\right)^{-1} \qquad \text{for } p = 2, \tag{13}$$

(Tarantola, 1987) where $G_{ij} = \partial g_i / \partial m_j$. This formula is only approximate because the problem is nonlinear. No formula for $\mathbf{C}_{M'}$ exists when $1 \leq p < 2$, but this relation may still be used for a crude estimate of $\mathbf{C}_{M'}$. Second, the elements of the resolution matrix,

$$\mathbf{R} = \mathbf{I} + \mathbf{C}_{M'} \mathbf{C}_M^{-1} \quad , \tag{14}$$

are examined to determined how well the parameters (or a linear combination of parameters) are resolved. When a diagonal element of $\mathbf{R}$ is close to 1, the corresponding parameter is well resolved; but, when it is close to 0, the parameter is poorly resolved. Because the resolution matrix strictly applies to undamped, linear problems with $p = 2$, the matrix for this highly damped, nonlinear problem with $p = 1$ is severely distorted. Third, the Jacobian matrix for the optimal model parameters is examined to determine how strongly the wavenumbers, l, depend upon the elastic moduli at each

frequency. The elements are normalized,

$$\frac{m_i}{l}\frac{\partial l}{\partial m_i} \quad ,$$

to make them nondimensional. The sensitivity can be interpreted as the percent change in the wavenumber due to a one percent change in a modulus.

RESULTS AND DISCUSSION

Hard Formation

An accurate estimate for c_{66} but poor estimates for c_{11} and c_{13} were obtained from the synthetic data for the hard formation. Using the Green River Shale (Thomsen, 1986) as the formation in the borehole model, synthetic seismograms were calculated (Figure 3) and were processed to obtain wavenumber and amplitude estimates at many frequencies (Figure 4). The initial model parameters and standard deviations were selected from the cross-plots (Figure 2) and are listed in Table 2. The initial modulus for the fluid, λ, corresponds to an acoustic velocity of 1500 m/s, and its standard deviation to an equivalent deviation in velocity of 38 m/s. p was selected to be 1. The final model parameters and standard deviations are also listed in Table 2. The estimate for c_{66} is fairly close to its correct value, but those for c_{11} and c_{13} are even less accurate than their initial values. The value for the fluid modulus did not change because the standard deviation is very small. The estimate for c_{66} using a least-squares inversion ($p = 2$) was slightly less accurate than the result presented here.

The initial and final standard deviations, the resolution matrix, and the sensitivities show that the inversion resolves c_{66} and λ moderately well but c_{11} and c_{13} poorly. Comparing the initial and final standard deviations suggests that c_{11} and c_{66} are moderately well resolved whereas c_{13} and λ are poorly resolved. The resolution matrix (Table 3) indicates that c_{66} is moderately well resolved but that the other moduli are

	Model Parameters			Standard Deviations	
Moduli	initial	final	correct	initial	final
c_{11}	3.00	2.68	3.13	1.00	0.729
c_{13}	1.10	4.14×10^{-3}	0.345	2.00	1.98
c_{66}	1.00	0.892	0.882	0.500	0.341
λ	0.225	0.225	0.225	1.50×10^{-4}	1.50×10^{-4}

Table 2: Initial and final parameters of the inversion for the hard formation.

	c_{11}	c_{13}	c_{66}	λ
c_{11}	0.066	0.015	0.88	31.
c_{13}		0.17	0.21	3.7
c_{66}			0.47	0.17
λ				6.7×10^{-5}

Table 3: Resolution matrix from the inversion for the hard formation. The matrix is highly distorted.

poorly resolved. Only the upper triangle of the resolution matrix is displayed because it is symmetric. The resolution matrix is highly distorted for two reasons: (1) the damping is severe (i.e., the element in $\mathbf{C}_M$ associated with the fluid elastic modulus is small compared to the elements $\mathbf{C}_D$); and (2) $\mathbf{C}_{M'}$, which is used to calculate $\mathbf{R}$, is very crude because $p = 1$. Because c_{11} and c_{66} are highly correlated (Table 1) the linear combination of these two parameters is well resolved. Furthermore, the changes to c_{66}, which are large because the data are moderately sensitive to this modulus, cause corresponding changes to c_{11}. The resulting improvement in the standard deviation falsely indicates that this parameter is well resolved. The sensitivities (Figure 5) show that the data should resolve λ well and c_{66} moderately well but not the other moduli. (The sensitivities for c_{33} and c_{44} are also shown, but since these parameters are fixed they will not affect the inversion.) For the tube wave, the effects of λ and c_{66} on the wavenumber are important at low frequencies but diminish as the frequency increases. Elastic constants c_{11} and c_{13} have little influence on the wavenumber for the tube wave. For the pseudo-Rayleigh wave, the wavenumber is affected by λ at high frequencies but is virtually unaffected by the other moduli. Despite the sensitivity of the wavenumber data to λ, the sensitivity is not large enough to decrease the very small standard deviation. For the same reason, the diagonal element in the resolution matrix associated with λ is small.

Soft Formation

The synthetic data from the soft formation yielded an accurate estimate for c_{66} but poor estimates for c_{11} and c_{13}. Shale (5000) (Thomsen, 1986) was used as the formation in the borehole model. The procedures for generating the synthetic seismograms (Figure 6), processing the seismograms to obtain wavenumber and amplitude estimates (Figure 7), and performing the inversion (Table 4) are the same as those used for the hard formation. The estimate for c_{66} is fairly close to its correct value. The improvement in c_{11} results from its strong correlation with c_{66}. That is, c_{66} must increase from

Moduli	Model Parameters			Standard Deviations	
	initial	final	correct	initial	final
c_{11}	3.00	3.06	3.40	1.00	0.995
c_{13}	0.900	0.128	1.06	2.00	2.00
c_{66}	0.900	1.03	1.05	0.500	0.497
λ	0.225	0.225	0.225	1.50×10^{-4}	1.50×10^{-4}

Table 4: Initial and final parameters of the inversion for the soft formation.

	c_{11}	c_{13}	c_{66}	λ
c_{11}	3.9×10^{-4}	5.9×10^{-5}	2.0×10^{-2}	3.8×10^{-1}
c_{13}		1.4×10^{-5}	1.9×10^{-3}	3.4×10^{-2}
c_{66}			1.1×10^{-2}	2.1×10^{-1}
λ				3.6×10^{-7}

Table 5: Resolution matrix from the inversion for the soft formation. The matrix is highly distorted.

its initial to its final value, and the large correlation coefficient makes c_{11} increase also. Like the inversion for the hard formation, the estimate for c_{13} is poor, and the estimate for λ did not change. The l_2 inversion yielded similar, but slightly less accurate results.

Elastic moduli, c_{66} and λ, are well resolved, but the others are poorly resolved. Comparing the initial and final standard deviations suggests that all moduli are poorly resolved. Similarly the resolution matrix, although it is distorted by damping and the reweighting matrix, also indicates that all parameters are poorly resolved. However, the sensitivities (Figure 8) for the tube wave suggest that some moduli are actually better resolved. The wavenumber data are greatly affected by λ and c_{66} at low frequencies but their influence diminishes as the frequency increases. The effect of c_{11} and c_{13} on the wavenumber is small at all frequencies.

CONCLUSIONS

The inversions performed on the synthetic data from the hard and soft formations had similar results. The estimate of c_{66} was reasonably accurate whereas those for c_{11} and c_{13} were poor. In fact, the cross-plots seem to give better estimates of c_{11}

and c_{13} than the inversion. The tight constraint on λ prevented this parameter from changing much. The interpretation of these results is difficult for two reasons: (1) the final model covariance matrix, $\mathbf{C}_{M'}$, is distorted by the reweighting matrix for the data, $\mathbf{W}$, and by the nonlinearity of the problem and (2) the resolution matrix, $\mathbf{R}$, which is calculated from $\mathbf{C}_{M'}$, is corrupted by the same problems that affect $\mathbf{C}_{M'}$ and by the severe damping. Nonetheless, the resolution of the model parameters can be roughly ascertained by examining the initial and final standard deviations, the resolution matrix, and sensitivities. In both the hard and the soft formations, c_{66} and λ are moderately well resolved by the data, and c_{11} and c_{13} are poorly resolved.

ACKNOWLEDGEMENTS

This work was supported by the Full Waveform Acoustic Logging Consortium at M.I.T. K. J. Ellefsen is partially supported by the Phillips Petroleum Fellowship.

REFERENCES

Aki, K. and P. G. Richards, *Quantitative Seismology,* W. H. Freeman & Co., 1980.

Auld, B. A., *Acoustic Fields and Waves in Solids,* vol. 1, John Wiley & Sons, Inc., 1973.

Bard, Y., *Nonlinear Parameter Estimation,* Academic Press Inc., 1974.

Burns, D. R., Viscous fluid effects on guided wave propagation in a borehole, *J. Acoust. Soc. Am., 83,* 463–469, 1988.

Chan, A. K. and L. Tsang, Propagation of acoustic waves in a fluid-filled borehole surrounded by a concentrically layered transversely isotropic formation, *J. Acoust. Soc. Am., 74,* 1605–1616, 1983.

Cheng, C. H., Full waveform inversion of P waves for V_s and Q_p, *M.I.T. Full Waveform Acoustic Logging Consortium Annual Report,* 323–338, 1987.

Cheng, C. H., M. N. Toksöz, and M. E. Willis, Determination of in situ attenuation from full waveform acoustic logs, *J. Geophys. Res., 87,* 5477–5484, 1982.

Ellefsen, K. J. and C. H. Cheng, Applications of perturbation theory to acoustic logging, *M.I.T. Full Waveform Acoustic Logging Consortium Annual Report,* 7–32, 1989.

Ellefsen, K. J., C. H. Cheng, and G. L. Duckworth, Estimating phase velocity and attenuation of guided waves in acoustic logging data, *M.I.T. Full Waveform Acoustic Logging Consortium Annual Report,* 405–419, 1987.

Meredith, J. A., R. H. Wilkens, and C. H. Cheng, Evaluation and prediction of shear wave velocities in soft marine sediments, *M.I.T. Full Waveform Acoustic Logging Consortium Annual Report,* 1989.

Moré, J. J., The Levenberg-Marquardt algorthim: Implementation and theory, in *Lecture Notes in Mathematics, no. 630,* edited by G. A. Watson, pp. 105–116, Springer-Verlag, 1978.

Moré, J. J., B. S. Garbow, and K. E. Hillstrom, *Users Guide for Minpack-1,* Argonne National Laboratory, 1982.

Rosenbaum, J. H., Synthetic microseismograms: Logging in porous formations, *Geophysics, 39,* 14–32, 1974.

Scales, J. A. and A. Gersztenkorn, Robust methods in inverse theory, *Inverse Problems, 4,* 1071–1091, 1988.

Stevens, J. L. and S. M. Day, Shear velocity logging in slow formations using the Stoneley wave, *Geophysics, 51,* 137–147, 1986.

Tarantola, A., *Inverse Problem Theory,* Elsevier Science Publ. Co., Inc., 1987.

Thomsen, L., Weak elastic anisotropy, *Geophysics, 51,* 1954–1966, 1986.

Tongtaow, C., *Wave Propagation along a Cylindrical Borehole in a Transversely Isotropic Formation,* Ph.D. thesis, Colorado School of Mines, 1982.

White, J. E. and C. Tongtaow, Cylindrical waves in transversely isotropic media, *J. Acoust. Soc. Am., 70,* 1147–1155, 1981.

Winterstein, D. F., Anisotropy effects in P-wave and SH-wave stacking velocities contain information on lithology, *Geophysics, 51,* 661–672, 1986.

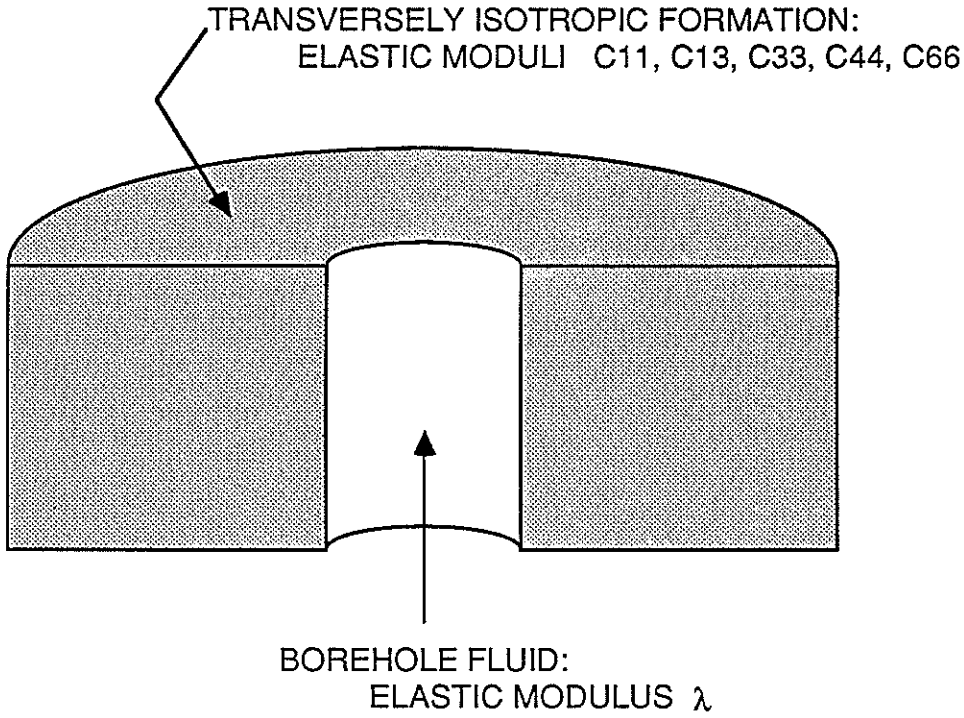

Figure 1: Borehole model used for the inversion.

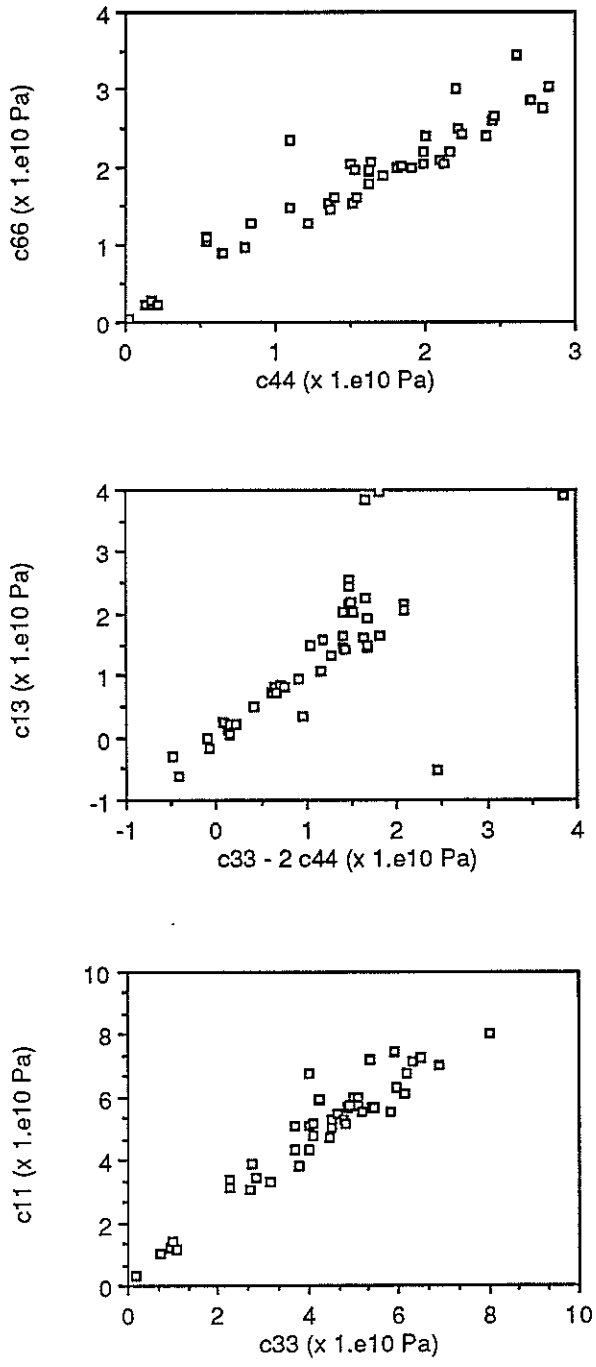

Figure 2: Cross-plots of elastic moduli tabulated by Thomsen (1986).

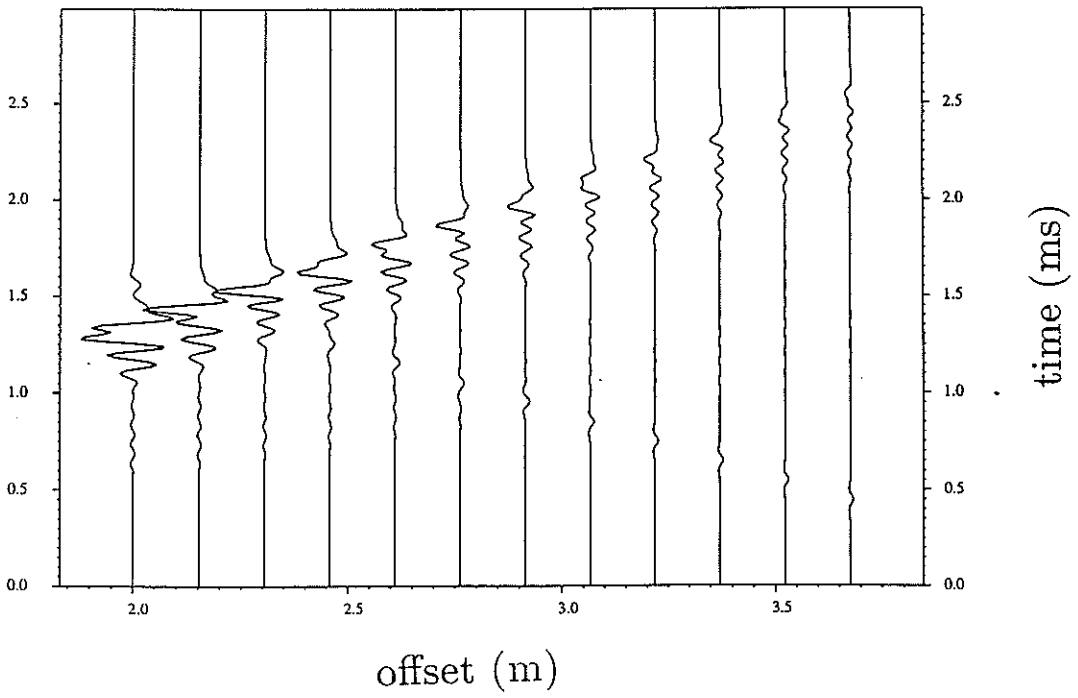

Figure 3: Synthetic microseismograms for the hard formation.

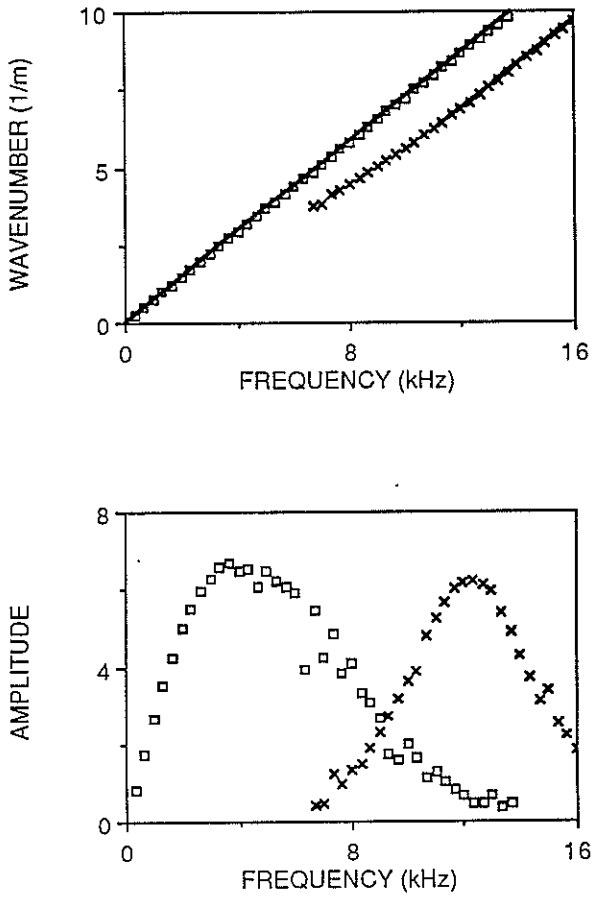

Figure 4: Wavenumber and amplitude estimates obtained by processing the synthetic microseismograms for the hard formation. The estimates for the tube wave are shown with a square, and those for the pseudo-Rayleigh wave with an "x". The wavenumbers predicted by the final model are shown by the solid line.

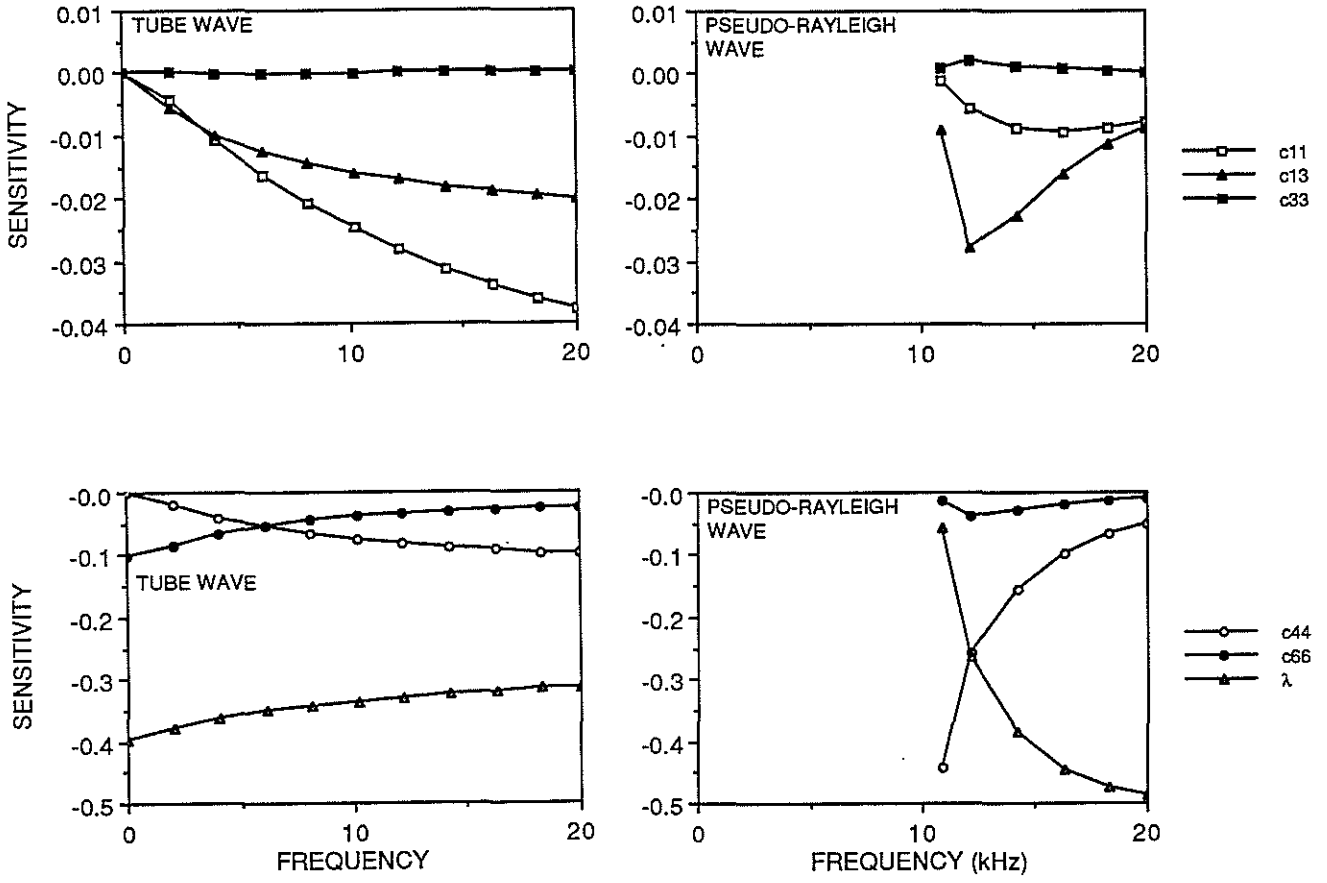

Figure 5: Sensitivities for the tube and pseudo-Rayleigh waves in the hard formation. Because the sensitivities for c_{11}, c_{13}, and c_{33} are much smaller than the other sensitivities, they are grouped together and plotted at a different scale.

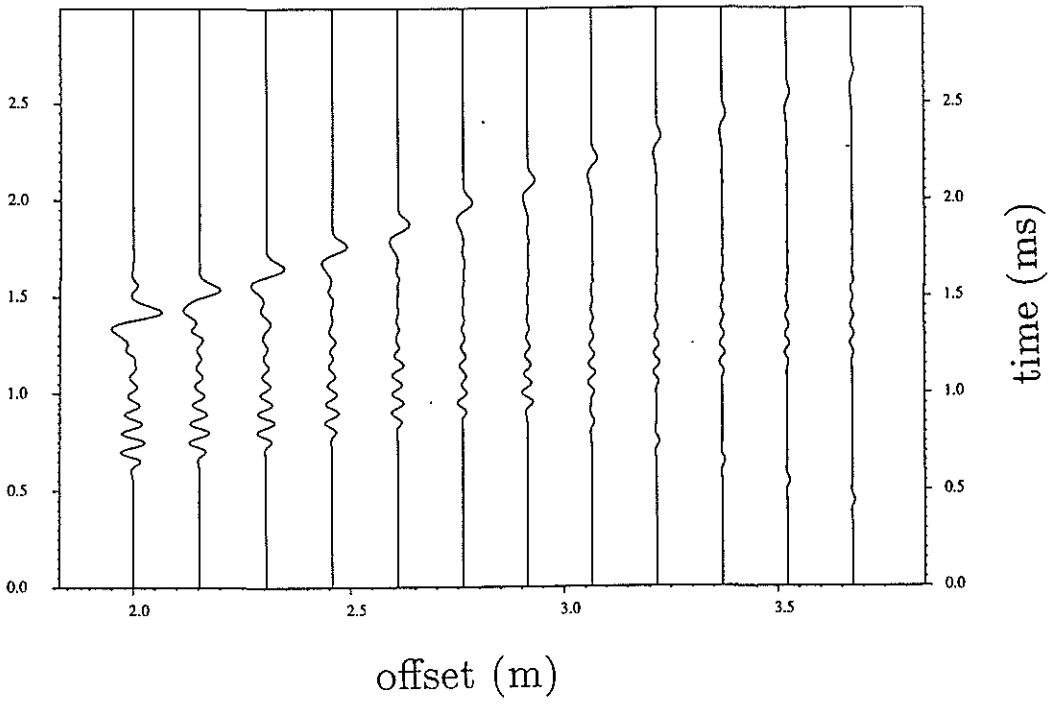

Figure 6: Synthetic microseismograms for the soft formation.

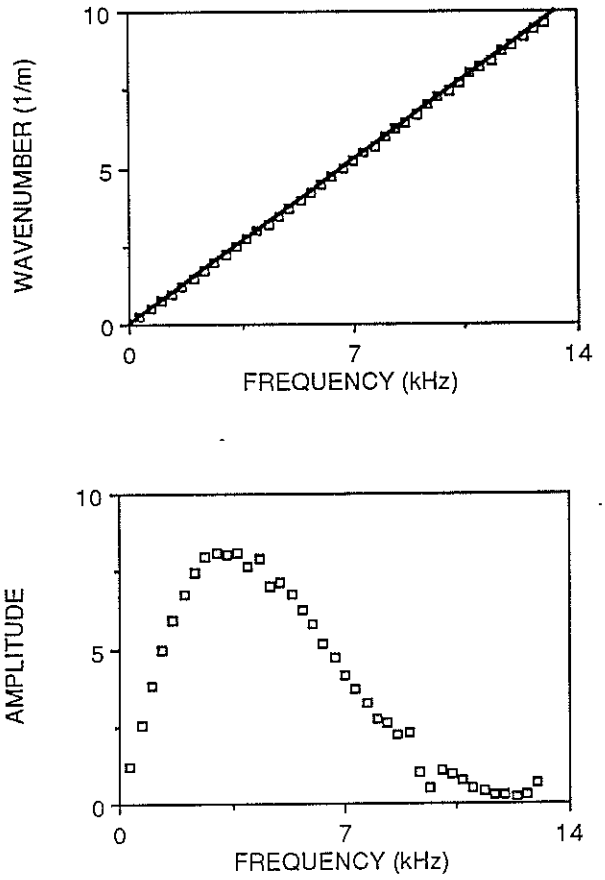

Figure 7: Wavenumber and amplitude estimates obtained by processing the synthetic microseismograms for the soft formation. The wavenumbers predicted by the final model are shown by the solid line.

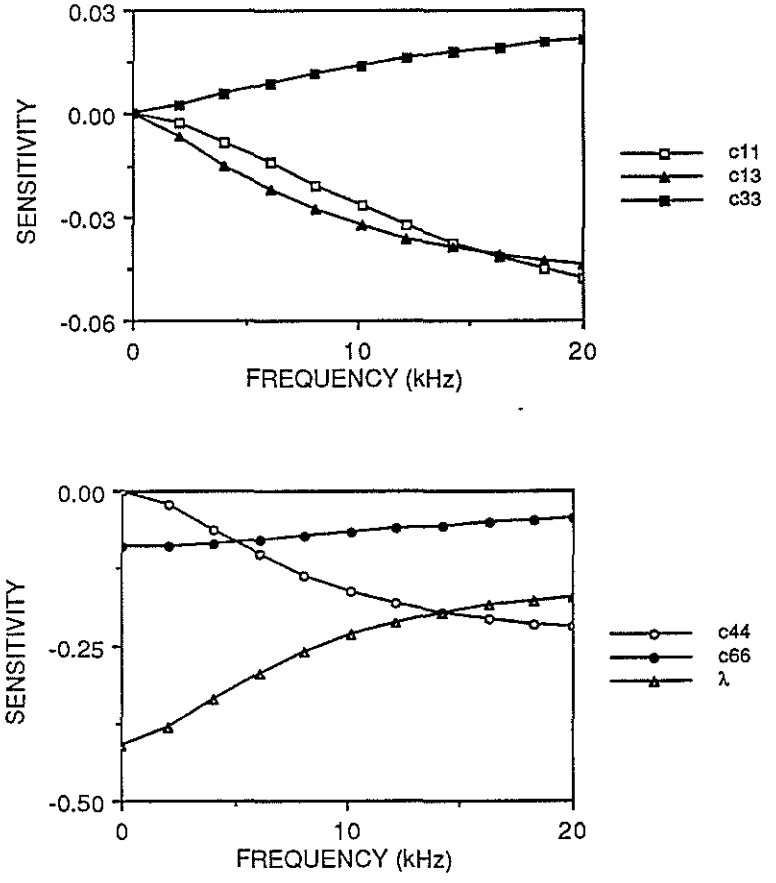

Figure 8: Sensitivities for the tube wave in the soft formation.